

# Spherical Colloids: Effect of Discrete Macroion Charge Distribution and Counterion Valence

René Messina

*Max-Planck-Institut für Polymerforschung, Ackermannweg 10 55128, Mainz, Germany*

---

## Abstract

We report the coupled effects of macroion charge discretization and counterion valence in the primitive model for spherical colloids. Instead of considering a uniformly charged surface, as it is traditionally done, we consider a more realistic situation where *discrete monovalent microscopic charges* are randomly distributed over the sphere. Monovalent or multivalent counterions ensure global electroneutrality. We use molecular dynamics simulations to study these effects at the ground state and for finite temperature. The ground state analysis concerns the counterion structure and *charge inversion*. Results are discussed in terms of simple analytical models. For finite temperature, strong and weak Coulomb couplings are treated. In this situation of finite temperature, we considered and discussed the phenomena of ionic pairing (pinning) and unpairing (unpinning).

*Key words:* Charged colloids, charge inversion, order-disorder transformations, molecular dynamics

*PACS:* 82.70.Dd, 61.20.Qg, 64.60.Cn

---

## 1 Introduction

Charged colloidal suspensions are a subject of intense experimental and theoretical work, and this, not only because of their direct application in industrial or biological processes, but also because they represent *model* systems. The electrostatic interactions involved in such systems have a fundamental role in determining the physico-chemical properties of such materials [1,2]. Theoretical description of highly charged colloidal solutions faces two challenges: (i) multi-length scale spatial correlations due to the presence of macroions (i.

---

*Email address:* [messina@mpip-mainz.mpg.de](mailto:messina@mpip-mainz.mpg.de) (René Messina).

e. charged colloids of the size 10-1000 Å) and microscopic counterions and (ii) their *long-range* Coulomb interaction. A first simplifying assumption is to treat the solvent as a dielectric medium solely characterized by its relative permittivity  $\epsilon_r$ . A second widely used approximation consists in modeling the *short range* ion-ion excluded volume interaction by hard spheres. These two approximations are the basis of the so-called primitive model of electrolyte solutions. The system under consideration is an asymmetrical electrolyte solution made up of highly charged macroions and small counterions. A further simplification, motivated by this asymmetry, can be made by partitioning the system into subvolumes (cells), each containing one macroion together with its neutralizing counterions plus, if present, additional salt. This approximation has been called accordingly the cell model [3,4]. The cells assume the symmetry of the macroion, here spherical, and are electrostatically decoupled. It is within the cell model that we present our simulation results.

For spherical macroions the structural charge is usually modeled by a *central charge*, which, by Gauss theorem, is equivalent to considering a *uniform* surface charge density as far as the electric field (or potential) *outside* the spherical colloid is concerned.

Most analytical concepts as well as simulations rely on the above assumptions especially on the central charge assumption. It is well known that in the strong Coulomb coupling regime ion-ion correlations become very important, and significant deviations from mean-field approaches are expected. A counter-intuitive effect which classical mean-field theories (like Poisson-Boltzmann model) cannot explain is the phenomenon of *overcharge*, also called charge inversion. That is, there are counterions in *excess* in the vicinity of the macroion surface so that its net charge changes sign. This has recently attracted significant attention [5–17]. In particular, we showed recently that this phenomenon may give rise to a strong long range attraction between like-sign charged colloids [12,13,17]. A natural question which comes up is: does overcharge and more generally ion-ion correlations strongly depend on the way the macroion structural charge is represented (i. e. uniformly charged or discrete charges on its surface)? In a recent paper [16], we studied such a situation in the strong Coulomb coupling regime where the macroion charge was carried by divalent microions in the presence of divalent counterions (*same* ionic valence). In Ref. [16] we reported the important result showing that overcharge is still possible under those conditions. More over we showed that that the intrinsic electric field solely due to the macroion surface microions (without counterions) varies strongly from point to point on the colloidal sphere [16].

The goal of this paper is to study, by means of molecular dynamics (MD) simulations, the *coupled* effects of macroion charge discretization and counterion valence in the primitive model for spherical colloids. A systematic comparison with the continuous macroion charge density (i. e. central charge) is under-

taken. The paper is organized as follows. In Sec. 2 we give some details on the macroion charge discretization as well as on the MD simulation model. Section 3 is devoted to the the ground state analysis where surface counterion structure and overcharge are addressed. In Sec. 4 we investigate the finite temperature situation, where counterion structure is studied for the strong and weak Coulomb couplings. Finally, in Sec. 5 we provide a summary of the results.

## 2 Simulation model

### 2.1 Macroion charge discretization

The procedure is similar to the one used in a previous study [16]. The *discrete* macroion charge distribution is produced by using  $Z_m$  *monovalent* microions of diameter  $\sigma$  (same diameter as the counterions), distributed *randomly* on the surface of the macroion. Then the structural charge is  $Q = -Z_m e = -Z_m Z_d e$ , where  $Z_m > 0$ ,  $Z_d = 1$  is the valence of these discrete microions and  $e$  is the positive elementary charge. These discrete colloidal charges (DCC) are *fixed* on the surface of the spherical macroion. Figure 1 shows a schematic view of the setup. The counterions (not shown in Fig. 1) have a charge  $q = +Z_c e$ , where  $Z_c > 0$  stands for the counterion valence. In spherical coordinates the elementary surface is given by:

$$dA = r_0^2 \sin \theta d\theta d\varphi = -r_0^2 d(\cos \theta) d\varphi, \quad (1)$$

where  $r_0$  is the distance between the macroion center and the DCC center. Thus to produce a random discrete charge distribution on the surface we generated (uniformly) randomly the variables  $\cos \theta$  and  $\varphi$ . Excluded volume is taken into account by rejecting configurations leading to an overlap of microions. Phenomena such as surface chemical reactions [18], hydration, roughness [19] are not considered. For commodity we introduce the notation  $(-Z_d : +Z_c)$  to characterize the valence symmetry (asymmetry) for  $Z_c = 1$  (for  $Z_c > 1$ ) of the ions (DCC and counterions) involved in discrete systems.

### 2.2 Molecular dynamics procedure

A molecular dynamics (MD) simulation technique was used to compute the motion of the counterions coupled to a heat bath acting through a weak stochastic force  $\mathbf{W}(t)$ . The procedure is very similar to the one used in previous studies [12,16].

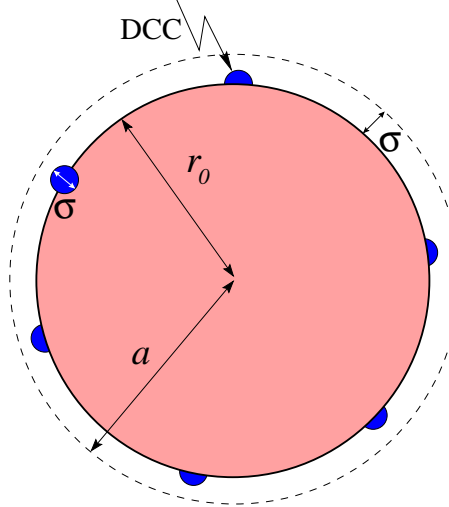


Fig. 1. Schematic view of the setup: the discrete colloidal charges (DCC) of diameter  $\sigma$  are in dark grey. For a detailed meaning of the other symbols see text. Note that this is a two-dimensional representation of the three-dimensional system.

The motion of counterion  $i$  (DCC ions being *fixed*) obeys

$$m \frac{d^2 \mathbf{r}_i}{dt^2} = -\nabla_i U(\mathbf{r}_i) - m\gamma \frac{d\mathbf{r}_i}{dt} + \mathbf{W}_i(t), \quad (2)$$

where  $m$  is the counterion mass,  $U$  is the potential force having two contributions: (i) the Coulomb interaction and (ii) the excluded volume interaction, and  $\gamma$  is the friction coefficient. Friction and stochastic force are linked by the dissipation-fluctuation theorem  $\langle \mathbf{W}_i(t) \cdot \mathbf{W}_j(t') \rangle = 6m\gamma k_B T \delta_{ij} \delta(t - t')$ . For the ground state simulations the stochastic force is set to zero.

Excluded volume interactions are taken into account with a pure repulsive Lennard-Jones potential given by

$$U_{LJ}(r) = \begin{cases} 4\epsilon_{LJ} \left[ \left( \frac{\sigma}{r-r_0} \right)^{12} - \left( \frac{\sigma}{r-r_0} \right)^6 \right] + \epsilon_{LJ}, & \text{for } r - r_0 < r_{cut}, \\ 0, & \text{for } r - r_0 \geq r_{cut}, \end{cases} \quad (3)$$

where  $r_0 = 0$  for the microion-microion interaction (the microion being either a counterion or a DCC),  $r_0 = 7\sigma$  for the macroion-counterion interaction, and  $r_{cut} (= 2^{1/6}\sigma)$  is the cutoff radius. This leads to a macroion-counterion distance of closest approach  $a = 8\sigma$  (see also Fig. 1). The macroion surface charge density  $\sigma_m$  is defined as

$$\sigma_m = \frac{Z_m}{4\pi a^2}. \quad (4)$$

Table 1  
Simulation parameters with some fixed values.

parameters	
$\sigma = 3.57 \text{ \AA}$	Lennard Jones length units
$T_0 = 298K$	room temperature
$\epsilon_{LJ} = k_B T_0$	Lennard Jones energy units
$Z_m$	macroion valence
$Z_d = 1$	discrete colloidal charge valence
$Z_c$	counterion valence
$l_B$	Bjerrum length
$a = 8\sigma$	macroion-counterion distance of closest approach
$\sigma_m$	macroion surface charge density
$R = 40\sigma$	simulation cell radius
$f_m = 8 \times 10^{-3}$	macroion volume fraction

Energy and length units in our simulations are related to experimental units by taking  $\epsilon_{LJ} = k_B T_0$  (with  $T_0 = 298 \text{ K}$ ), and  $\sigma = 3.57 \text{ \AA}$  respectively.

The pair electrostatic interaction between any pair  $ij$ , where  $i$  and  $j$  denote either a DCC a counterion or the central charge (for the non-discrete case), reads

$$U_{coul}(r) = k_B T_0 l_B \frac{Z_i Z_j}{r}, \quad (5)$$

where  $l_B = e^2 / 4\pi\epsilon_0\epsilon_r k_B T_0$  is the Bjerrum length describing the electrostatic strength.

The macroion and the counterions are confined in a spherical impenetrable cell of radius  $R$ . The macroion is held fixed and is located at the center of the cell. The colloid volume fraction  $f_m$  is defined as  $a^3/R^3$ . To avoid image charge complications, the permittivity  $\epsilon_r$  is supposed to be identical within the whole cell (including the macroion) as well as outside the cell. Typical simulation parameters are gathered in Table 1.

### 3 Ground state analysis

In this section, we focus on counterion distribution exclusively governed by *energy minimization*, i. e.  $T = 0K$ . In such a case correlations are maximal, and

all the counterions lie on the surface of the spherical macroion. This situation has the advantage to enable accurate computation of energy variations in such processes as overcharging and also to clearly understand effects which are purely correlational in nature. The method employed here was successfully carried out in Refs. [12,13,16,17] and is explained in details in Ref. [17]. The Bjerrum length  $l_B$  is set to  $10\sigma$ . Note that in the ground state the value of  $l_B$ , or equivalently the value of the dielectric constant  $\epsilon_r$ , does not influence at all the counterion structure, only the electrostatic energy is rescaled accordingly.

### 3.1 Neutral case

First we consider the simple case where the system [macroion + counterions] is globally neutral. In order to characterize the two-dimensional counterion structure, we compute the counterion correlation function (CCF)  $g_c(r)$  on the surface of the sphere, defined as:

$$c^2 g_c(r) = \sum_{i \neq j} \delta(r - r_i) \delta(r - r_j), \quad (6)$$

where  $c = N_c/4\pi a^2$  is the surface counterion concentration ( $N_c = Z_m/Z_c$  being the number of counterions),  $r$  corresponds to the arc length on the sphere. Note that at zero temperature all equilibrium configurations are identical (except for exceptional accidental degenerate ground state), thus only one is required to obtain the  $g_c(r)$ . Similarly, one can also define a surface macroion correlation function (MCF)  $g_m(r)$  for the microions (representing the colloidal structural charge) on the surface of the macroion. The counterion correlation function  $g_c(r)$  is normalized as follows

$$c \int_0^{\pi a} 2\pi r g_c(r) dr = (N_c - 1). \quad (7)$$

Because of the *finite* size and the topology of the sphere,  $g(r)$  has a cut-off at  $r_{gc} = \pi a = 25.1\sigma$  and  $g(r_{gc}) = 0$ . More precisely one can not set the uncorrelated case to  $g(r) = 1$  for the present finite system. Therefore at “large” distance the correlation function differs from the one obtained with a perfect infinite plane. Furthermore the absolute value of  $g(r)$  can not be directly compared to the one obtained with an infinite plane. The normalization of  $g_m(r)$  is very similar to Eq. (7) and reads

$$\sigma_m \int_0^{\pi a} 2\pi r g_m(r) dr = (Z_m - 1), \quad (8)$$

where the arc length has been rescaled by a factor  $a/r_0$  so that  $g_c(r)$  and  $g_m(r)$  are directly comparable (see also the setup Fig. 1) and are defined in the same  $r$  range.

### 3.1.1 Monovalent counterions

We first treat the systems where we have monovalent counterions, that is we have to deal with the symmetric discrete system (-1:+1). The counterion correlation functions  $g_c(r)$  are computed for a central macroion charge [denoted by  $g_c^{(CC)}(r)$ ] and for discrete macroion charge distribution [denoted by  $g_c^{(DCC)}(r)$ ]. Results for three structural charges  $Z_m = 60, 180$  and  $360$  are given in Figs. 2(a), (b) and (c) respectively. For the continuous case (central charge) a quasi Wigner crystal (WC) counterion structure is observed as was already found in Refs. [12,13,16,17]. Also the higher the absolute number of counterions  $N_c$  (i. e. the concentration  $c$ ) the higher the order of counterion structure for the continuous case [compare Fig. 2(a) with Fig. 2(c)].

It turns out that in the case of discrete colloidal charges the counterion distribution is strongly dictated by colloidal charge distribution, and this, especially for low macroion surface charge density  $\sigma_m$  ( $Z_m = 60$ ) [see Fig. 2(a)]. For  $Z_m = 60$ ,  $g_c^{(DCC)}(r)$  and  $g_m(r)$  are almost identical and this even for the first peak. This indicates that each counterion is exactly associated with one DCC site. In Fig. 3(a) is depicted the ground state structure for  $Z_m = 60$ , where one clearly observes this ionic pairing.

This strong ionic pair association can be easily explained in terms of *local* correlations. Let us consider the picture sketched in Fig. 4, which holds for strong ionic pairing, where a given dipole A (ionic pair made up of a counterion and a DCC site) of the macroion surface essentially interacts with its first nearest surrounding dipoles B. Note that very similar lengths were also considered in a recent theoretical study [20] in the one-dimensional case (counterion adsorption on a linear polyion). It is important to have in mind that such a local description is physically justified due to the strong screening generated by ionic pairing. Thereby local correlations are twofold: (i) the *attractive* interaction between the DCC site of dipole A with its paired counterion and the counterions of dipoles B, and (ii) the *repulsive* interaction between the counterion of dipole A and counterions of dipoles B. The correlations between DCC sites are not relevant since they are fixed. The intra-dipole attractive interaction  $E_{pin}$  between the DCC site and its “pinned” counterion can be written as

$$E_{pin} = -\frac{Z_d Z_c}{\sigma}. \quad (9)$$

For the elementary nearest inter-dipole (or inter-ionic pair) interactions, one

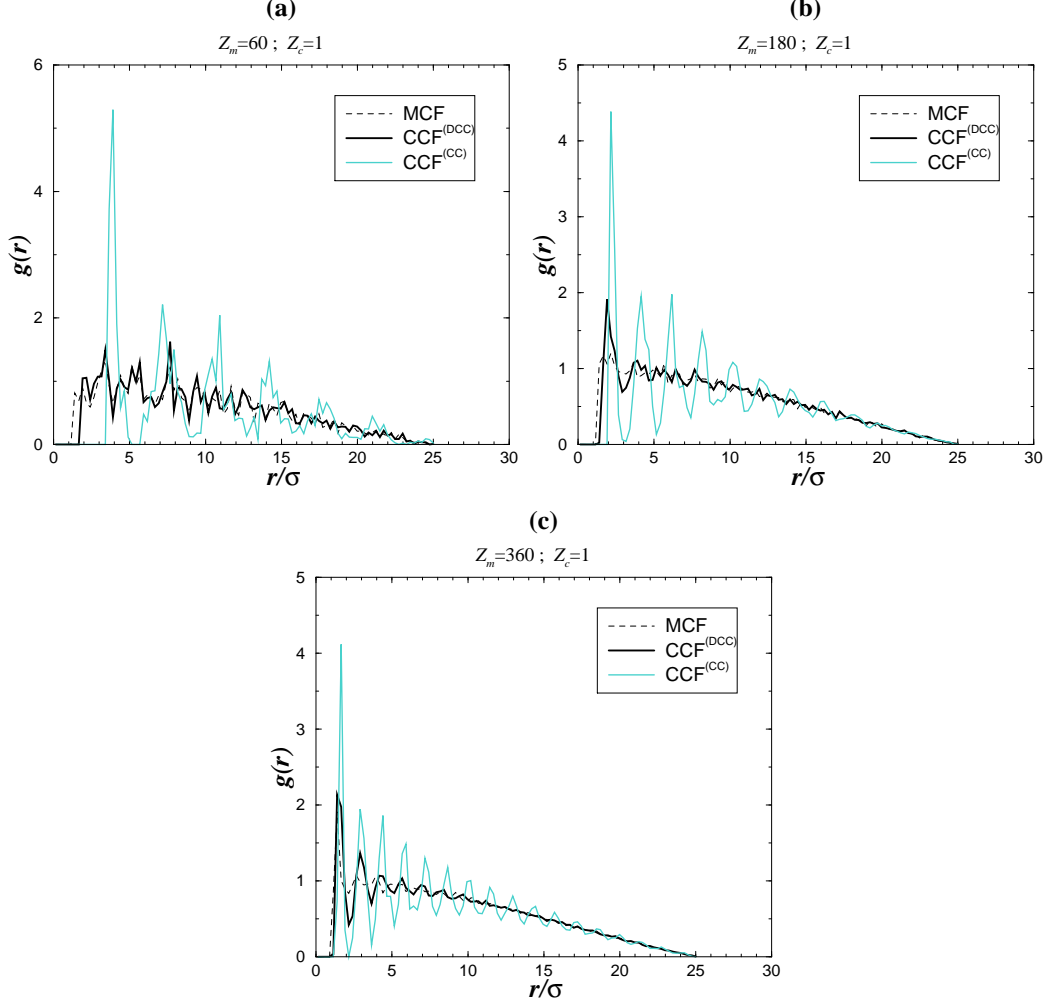


Fig. 2. Ground state surface correlation functions  $g(r)$  for *monovalent* counterions ( $Z_c = 1$ ) and for three macroion bare charges: (a)  $Z_m = 60$  (b)  $Z_m = 180$  and (c)  $Z_m = 360$ . The two counterion correlation functions (CCF)  $g_c(r)$  are obtained for discrete colloidal charges [ $g_c^{(DCC)}(r)$  denoted by  $CCF^{(DCC)}$ ] and for the central charge [ $g_c^{(CC)}(r)$  denoted by  $CCF^{(CC)}$ ]. MCF stands for the discrete colloidal charges pair distribution  $g_m(r)$ .

can write for the attractive interaction  $E_{+-}$  between the DCC site of dipole A and the counterion of dipole B:

$$E_{+-} = -\frac{Z_d Z_c}{a_{dc}}. \quad (10)$$

A similar expression can be written for the repulsive inter-dipole interaction  $E_{++}$  involving counterions of dipole A and dipole B, which reads

$$E_{++} = \frac{Z_c^2}{a_{cc}}. \quad (11)$$

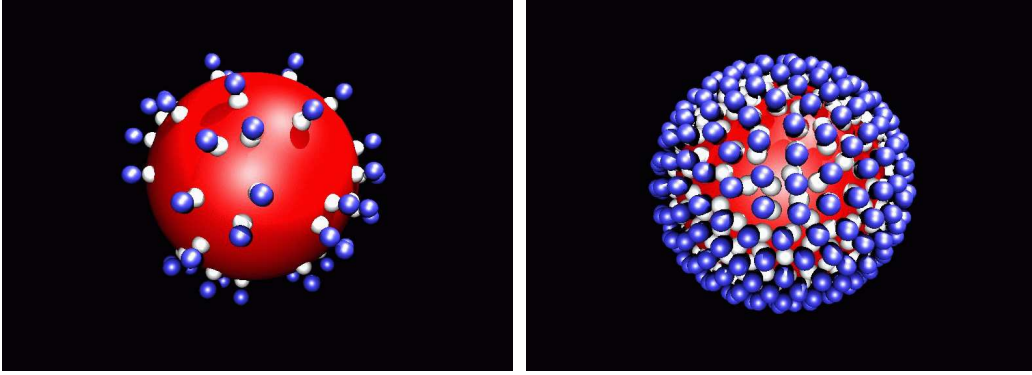


Fig. 3. Ground state structures for discrete monovalent systems (-1:+1): (a)  $Z_m = 60$  and (b)  $Z_m = 360$ . The discrete colloidal charges (DCC) are in white, and the counterions in blue. Full ionic pairing association occurs. The corresponding counterion correlation functions  $g_c(r)$  can be found in Figs. 2(a) and c).

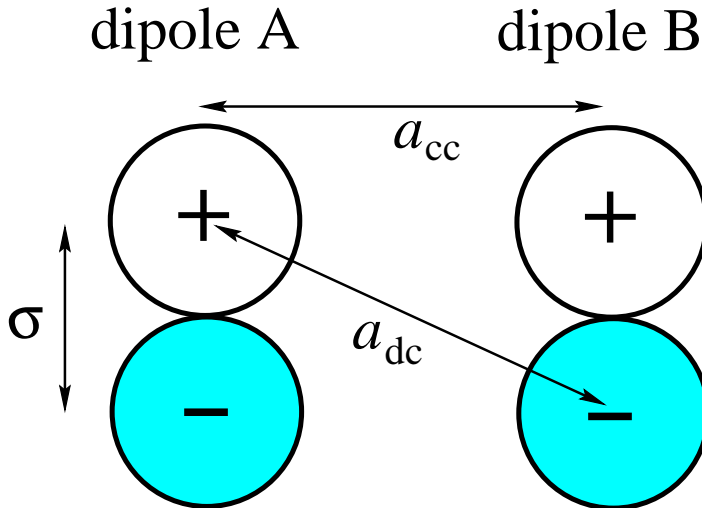


Fig. 4. Schematic view of the local electrostatic interactions and typical correlation lengths involved between nearest dipoles. The negatively charged DCC (-) are in grey and the positively charged counterions (+) in white.

Prefactor  $l_B k_B T_0$  has been omitted for clarity in Eqs. (9-11). Note that the repulsive counterion-counterion term  $E_{++}$  alone, even if space *truncated*<sup>1</sup>, drives to the *long-range* ordered triangular WC structure in the ground state for fixed surface counterion concentration  $c$ . However, at zero temperature the DCC sites represent pinning centers for the counterions where the electrostatic potential is considerably lowered (due to the term  $E_{pin}$ ) compared to its direct “empty” neighborhood (charge hole), which in turn prevents the counterions from adopting the ideal WC structure. This latter aspect was thoroughly discussed in Ref. [16]. Another important quantity characterizing

<sup>1</sup> This statement holds if the cutoff is larger than the lattice constant.

discrete systems is the ratio,

$$\rho_{pin} = \frac{\tilde{a}_{cc}}{d_{pin}}, \quad (12)$$

between the the mean inter-dipole separation  $\tilde{a}_{cc}$  (more exactly the mean counterion-counterion separation) and intra-dipole center-center separation  $d_{pin}$  of an ionic pair (in the present study  $d_{pin} = \sigma$  as depicted in Fig. 4). The value of  $\tilde{a}_{cc}$  can be obtained by taking the first peak position of  $g_c^{(CC)}(r)$ .

Obviously, for sufficiently low macroion surface charge density  $\sigma_m$  (i. e. large  $\rho_{pin}$ ), the ionic pairing term  $E_{pin}$  will be dominant and strong pinning (ionic pairing) occurs. More specifically, when the typical inter-dipole distance is large (i. e.  $a_{cc}$  or  $a_{dc}$  which are almost identical in this case) compared to the intra-dipole distance (here  $\sigma$ ), then dipole-dipole interactions are weak (i. e.,  $|E_{+-} - E_{++}| \ll |E_{pin}|$ ) and the DCC distribution dictates the counterion structure. This is what qualitatively explains our simulation findings for  $Z_m = 60$  [see Fig. 2(a) and Fig. 3(a)].

When the counterion concentration  $c$  (equivalently  $\sigma_m$ ) becomes sufficiently important the situation may become qualitatively different. In this case one has to be more careful concerning the typical distance between nearest ions. Indeed, by increasing  $\sigma_m$  (i. e. decreasing  $\rho_{pin}$ ), dipoles approach from each other, and because of excluded volume<sup>2</sup>  $a_{cc}$  becomes comparable to  $\sigma$  (see Fig. 4)<sup>3</sup>. Thereby, the counterion-counterion repulsion term  $E_{++}$  (overcompensating  $E_{+-}$ ) induces counterion ordering (so as to minimize their mutual repulsion) *compatible* with the local attractive pinning potential field generated by DCC centers. This effect can be inspected in Fig. 2(b) and Fig. 2(c) where one sees that upon increasing  $\sigma_m$ ,  $g_c^{(DCC)}(r)$  is gradually less correlated with  $g_m(r)$  and more correlated with  $g_c^{(CC)}(r)$ . As a topological consequence, some counterions will be in contact with several (two or more) DCC attractors. This topological feature can be seen in Fig. 3(b).

The quasi-triangular counterion arrangement for high  $\sigma_m$  ( $Z_m = 360$ ) can be inspected in Fig. 3(b). For this symmetric system in size (same diameter for the counterions and the DCC ions) one expects that, for a compact amorphous DCC layer, the counterion structure should become perfectly ordered. This extreme limit, which would correspond to unreachable experimental charge densities, has not been addressed in our simulations.

Note that in parallel, increasing  $\sigma_m$  induces, by excluded volume effect, a

<sup>2</sup> Note that in the present model no surface dipole flip is allowed which should also be the case experimentally.

<sup>3</sup> The limiting case is where the global structure is compact, i. e. touching spherical microions.

stronger local order within the DCC layer as can be checked on the  $g_m(r)$  plots in Figs. 2(a)-(c). This is quite similar to what occurs in a system of hard spheres where the (dense) liquid phase is locally correlated and the (dilute) gaseous phase is uncorrelated.

In summary, the system depicted above is the siege of an *order-disorder* phase transition, where, upon increasing  $\sigma_m$  (i. e. decreasing  $\rho_{pin}$ ), we pass from a disordered structure (imposed by the DCC layer) to a *long-range* ordered system induced by *local* counterion-counterion correlations.

Although results presented and discussed above concern one given random distribution (for each  $Z_m$ ), we carefully checked that similar results and conclusions could be drawn for different random realizations (systematically five). This holds also for the following section below where we deal with multivalent counterions.

### 3.1.2 Multivalent counterions

We turn to the asymmetric discrete systems ( $-1 : +Z_c$ ) where multivalent counterions are present ( $Z_c > 1$ ). The correlation functions  $g(r)$ , for two macroion charges  $Z_m = 60$  and  $Z_m = 180$  and various counterion valences  $Z_c$ , can be found in Fig. 5. One remarks that upon decreasing the number of counterions  $N_c$  (i.e. increasing  $Z_c$ ), for fixed  $Z_m$ , the first peak of  $g_c(r)$  is gradually shifted to the right (compare also the monovalent case given in Fig. 2), and this, whatever the nature of the macroion charge is (discrete or continuous). Indeed, due to Coulomb repulsion the counterions will try to stay apart as much as possible, and for the discrete case in competition with the DCC attractors. Furthermore, we observe for the discrete systems that upon increasing  $Z_c$ , for fixed  $Z_m$ , the correlation between  $g_c^{(DCC)}(r)$  and  $g_m(r)$  decreases and increases between  $g_c^{(DCC)}(r)$  and  $g_c^{(CC)}(r)$ . This effect is clearly noticeable in Fig. 2(b) and Figs. 5(c-e) corresponding to  $Z_m = 180$ . The very high counterion valence  $Z_c = 10$  reported in Fig. 5(e) was undertaken in order to stress the counterion multivalence effect. These findings lead to the important conclusion that the counterion valence has the effect of reducing the counterion structure disorder stemming from the DCC distribution randomness.

This related phenomenon can be theoretically explained with simple ideas. Basically, the mechanisms involved in this counterion valence induced ordering stem from two concomitant sources: (i) *topological* and (ii) *correlational*.

The topological aspect is due to the presence of  $(Z_m - Z_m/Z_c)$  unbound DCC sites (free of associated counterion) ensuring global electroneutrality [compare for instance Fig. 3(a) and Fig. 6]. This feature can be inspected in the snapshot for  $Z_c = 10$  in Fig. 6. It is to say that here, compared to the monovalent case (-1:+1), the counterions have much more “freedom” to choose their pinning

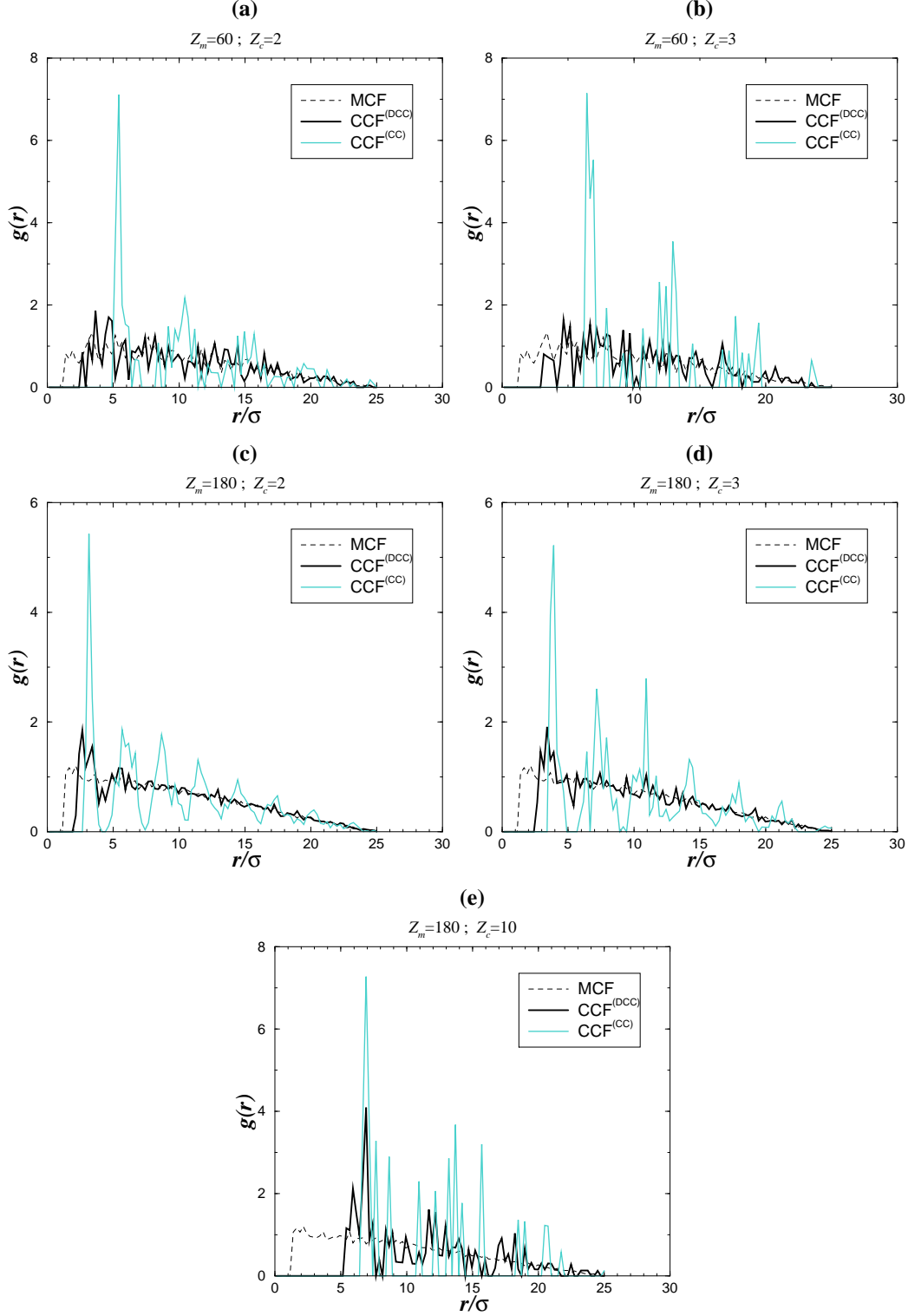


Fig. 5. Ground state surface correlation functions for different *multivalent* systems: (a)  $Z_m = 60$ ,  $Z_c = 2$ ; (b)  $Z_m = 60$ ,  $Z_c = 3$ ; (c)  $Z_m = 180$ ,  $Z_c = 2$ ; (d)  $Z_m = 180$ ,  $Z_c = 3$ ; (e)  $Z_m = 180$ ,  $Z_c = 10$ . The two counterion correlation functions (CCF) are obtained for discrete colloidal charges (DCC) and for the central charge (CC). The  $g_m(r)$  curves (denoted by MCF) are identical from (a) to (b) and from (c) to (e).

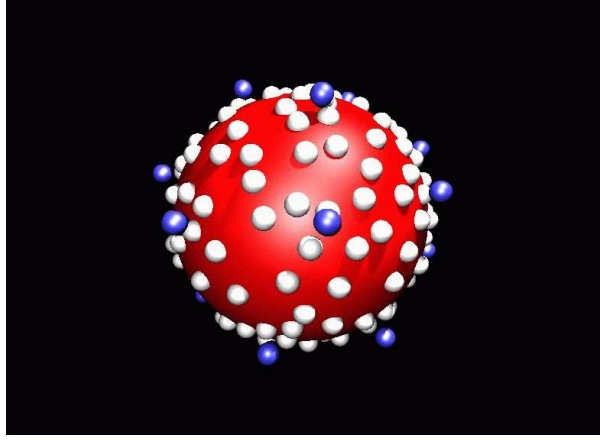


Fig. 6. Ground state structure for (-1:+10) with  $Z_m = 180$ . The corresponding counterion correlation function  $g_c(r)$  can be found in Figs. 5(e).

locations, and this, all the more  $Z_c$  is high. To be more precise, the number of topologically accessible “pinned” configurations is given <sup>4</sup> by

$$C_{Z_m}^{\frac{Z_m}{Z_c}} = \frac{Z_m!}{\left(Z_m - \frac{Z_m}{Z_c}\right)! \left(\frac{Z_m}{Z_c}\right)!} \quad (13)$$

which reduces to 1 for  $Z_c = 1$ . In the ground state, counterions will “decide” to choose among these various possible arrangements the one which minimizes the total energy of the system. It is clear that this topological feature, already alone, promotes counterion valence induced ordering.

Concomitantly, there is a purely counterion correlation induced ordering which is  $Z_c$  dependent. Indeed, using similar arguments as those previously employed for monovalent systems (-1:+1), built on Eqs. (9-11), one can infer the role of  $Z_c$ . More specifically, by assuming an ordered WC structure<sup>5</sup>, the term  $E_{++}$  given by Eq. (11) can be rewritten as

$$E_{++}^{WC} \sim \frac{Z_c^{3/2} Z_m^{1/2}}{a}, \quad (14)$$

where  $a_{cc}$  in Eq. (11) is now given by

$$a_{cc} = \tilde{a}_{cc} \sim c^{-1/2} \sim \left(\frac{Z_m}{Z_c a^2}\right)^{-1/2}. \quad (15)$$

<sup>4</sup> Rigorously, Eq. (13) holds when each counterion is associated with one and only one DCC site (case of low  $\sigma_m$ ). For high  $\sigma_m$ , it remains a good approximation to capture the essential physics.

<sup>5</sup> From a topology point of view, this corresponds to replace the actual (random) Voronoi structure by the ordered WC structure.

Equation (14) shows that, for fixed  $Z_m$  and  $a$  (i. e., fixed macroion charge density), the WC term  $E_{++}^{WC}$  scales like  $Z_c^{3/2}$  which means that, for high enough valence  $Z_c$ ,  $E_{++}^{WC}$  will be the dominant term, since  $E_{pin}$  scales like  $Z_c$  ( $Z_d = 1$  being fixed) and therefore with a weaker power. Thereby  $Z_c$  induces counterion ordering (so as to minimize their mutual repulsion), merely dictated by Eq. (14), *compatible* with the local attractive pinning potential field generated by DCC centers. As a topological consequence, some counterions, which would have been in contact with several DCC sites if they were monovalent, will now be in contact with less DCC sites. This topological feature can be seen in Fig. 6.

In summary, these discrete multivalent systems are again the siege of an order-disorder phase transition which is counterion valence controlled.

### 3.2 Overcharge

We now investigate the charge inversion (overcharge) phenomenon. The starting equilibrium configurations correspond to neutral ground states as were previously obtained. The method employed here is very similar to the one used in Refs. [12,16]. To produce controlled overcharge, one adds successively overcharging counterions (OC) at the vicinity of the macroion surface. Thereby the resulting system is no longer neutral. Using Wigner crystal concepts [6,21], we showed that the gain in electrostatic energy (compared to the neutral state) by overcharging a single *uniformly* charged macroion (i.e., central charge) with  $n$  overcharging counterions can be written in the following way [12,13,17]:

$$\Delta E_n^{OC} = \Delta E_n^{cor} + \Delta E_n^{mon} = -\frac{\alpha Z_c^2}{\sqrt{A}} \left[ (N_c + n)^{3/2} - N_c^{3/2} \right] + Z_c^2 \frac{n^2}{2a}, \quad (16)$$

where prefactor  $l_B k_B T_0$  has been omitted for clarity. As before  $N_c = Z_m/Z_c$  is the number of counterions in the neutral state,  $A$  is the macroion area ( $4\pi a^2$ ), and  $\alpha$  is a positive constant which was determined by using simulation data for  $\Delta E_1^{OC}$ .  $\Delta E_n^{cor}$ , which is equal to the first term of the right member, denotes the gain in energy due to ionic correlations. The derivation of this term can be found in Refs. [12,13,17], and the basic idea is that each counterion interacts essentially with its neutralizing uniformly charged Wigner-Seitz cell. The second term on the right hand side,  $\Delta E_n^{mon}$ , is the self-energy of the excess of charge. This repulsive term stops the overcharging for a sufficient high  $n$ . Note that the WC concept for describing energy correlations is already excellent for highly short range ordered structures (strongly correlated liquids, see Ref. [6] for a detailed discussion). The total electrostatic energy of the system as a function of  $n$  is displayed Fig. 7 (for monovalent counterions) and Fig. 8 (for multivalent counterions) for two bare charges  $Z_m = 60$  and

$Z_m = 180$ . The energy curves corresponding to discrete systems were produced by systematically averaging over five random DCC realizations. The resulting energy error bars are only indicated when larger than symbols.

### 3.2.1 Monovalent counterions

Let us first focus on the monovalent symmetric case (-1:+1) where for the neutral state each DCC site is exactly associated with one counterion as was shown above. Results in Figs. 7(a-b) clearly show that the overcharging process is quite different for these discrete “symmetric” monovalent systems (-1:+1) compared to the continuous case. Especially for the smallest bare charge  $Z_m = 60$ , the effect of disorder is very important in agreement with what was already found above for the neutral state in Sec. 3.2.1. The main effects of charge discretization are: (i) the reduction in gain of energy and (ii) the reduction of maximal (critical) number,  $n^*$ , of stabilizing overcharging counterions (corresponding to a minimum in energy curves). Both points were thoroughly discussed elsewhere [16] for an equivalent symmetric discrete system (-2:+2). It was shown that points (i) and (ii) can be explained in terms of *ion-dipole* interaction. It is exactly this *attractive* ion-dipole correlations which is responsible for the charge inversion for colloidal systems with discrete charges. When the overcharging counterions are present, each of them will essentially interact (attractively) with its neighboring dipoles (ionic pairs). The attractive ion-dipole interaction increases with decreasing ion-dipole separation, i. e. increasing colloid bare charge  $Z_m$  (i. e. charge density). This explains why the energy gained increases with  $Z_m$  [compare Fig. 7(a) and Fig. 7(b)]. On the other, the repulsion between the counterions is not fully minimized since they do not adopt the ideal Wigner crystal structure that is obtained with a central charge which in turn explains (i) and (ii). Note however that for high bare charge ( $Z_m = 180$ ) the overcharge curve obtained with DCC [see Fig. 7(b)] approaches the one from the continuous case as expected for high counterion concentration. This feature is fully consistent with what was already found in Sec. 3.1.1, where it was shown that the neutral ground state counterion structure order (for discrete systems) increases with  $\sigma_m$ . In other terms, the WC approach through Eq. (16) is a good approximation for describing discrete systems at high  $\sigma_m$  (since more ordered there).

Common features of overcharging between continuous and discrete systems are briefly given here. We note that  $n^*$  increases with the macroionic charge  $Z_m$ . Furthermore, for a given  $n$ , the gain in energy is always increasing with  $Z_m$ . Also, for a given macroionic charge  $Z_m$ , the gain in energy between two successive overcharged states is decreasing with  $n$ . Note that at  $T = 0K$ , the value  $\epsilon_r$  acts only as a prefactor. All these features are captured by Eq. (16).

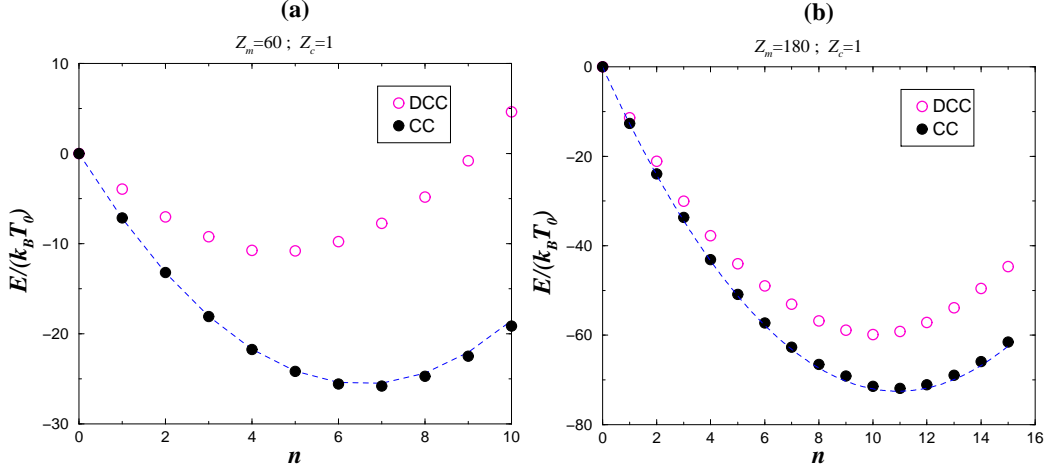


Fig. 7. Total electrostatic energy for *monovalent* counterions ground state configurations as a function of the number of *overcharging* counterions  $n$ : (a)  $Z_m = 60$  (b)  $Z_m = 180$ . Overcharge curves were computed for discrete macroion charge distribution (DCC) and central macroionic charge (CC). The neutral case was chosen as the potential energy origin. Dashed lines were produced by using equation (16). For discrete systems (DCC) error bars are smaller than symbols.

### 3.2.2 Multivalent counterions

Now we are going to discuss the asymmetric discrete systems ( $-1 : +Z_c$ ) where multivalent counterions are present ( $Z_c > 1$ ). Figures 8(a-d) clearly indicate that the energy gain in the overcharging process, at fixed  $Z_m$  and  $n$ , is higher the higher the counterion valence  $Z_c$ , and this for both macroion charge representations (discrete and continuous). For the continuous case (central charge) this can be directly explained in terms of WC concepts [i. e. Eq. (16)]. Indeed the main leading term of the correlational energy  $\Delta E_n^{cor}$  in Eq. (16) scales like

$$\Delta E_n^{cor} \sim -Z_c^{3/2} \quad (17)$$

for fixed  $n$  and fixed macroion charge  $Z_m$ , and recalling that  $N_c = Z_m/Z_c$ . Equation (17) quantitatively (qualitatively) explains why overcharging is stronger with increasing counterion valence  $Z_c$  for the continuous (discrete) case.

As far as discrete systems are concerned, the present situation (with  $Z_c > 1$ ), regarding overcharging mechanisms, differs from the symmetric monovalent systems ( $-1:+1$ ), because of the presence of  $(Z_m - Z_m/Z_c)$  unbound (free) DCC sites in the neutral state as discussed in Sec. 3.1.2. When overcharging comes into play, each overcharging counterion will become associated with

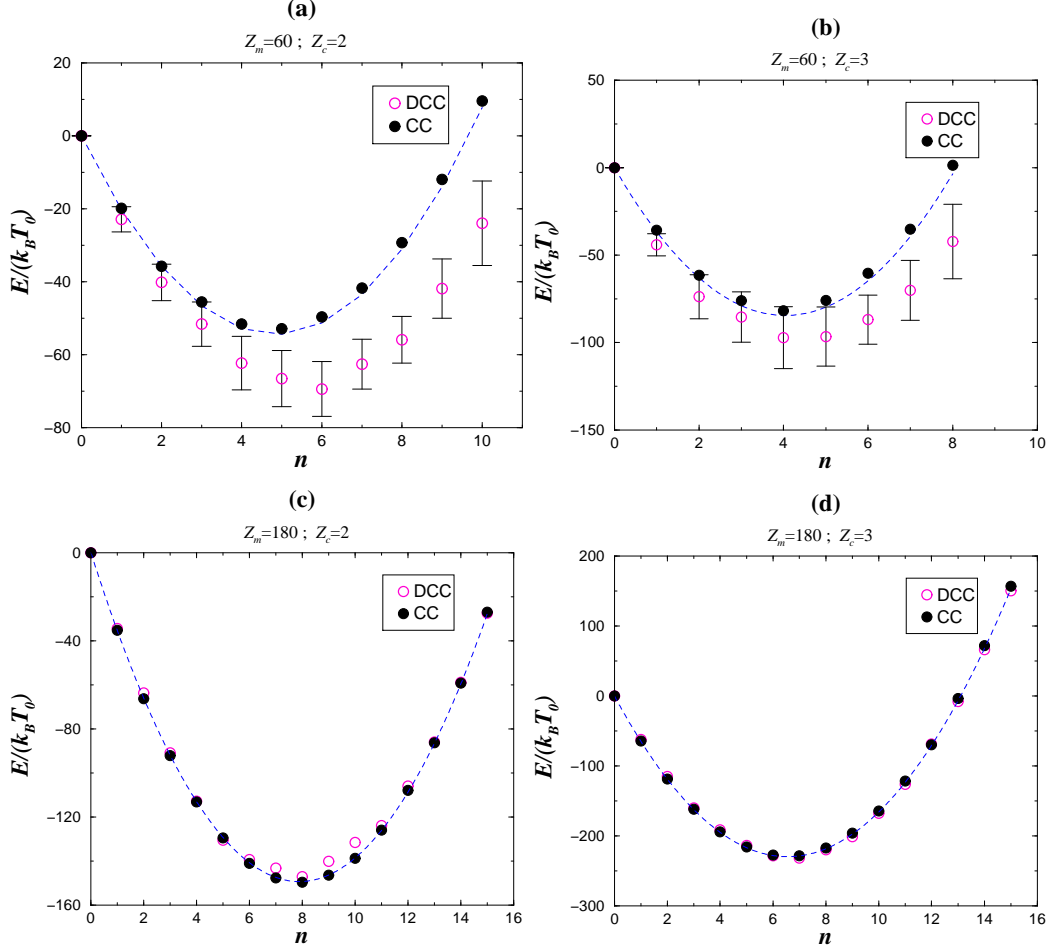


Fig. 8. Total electrostatic energy for *multivalent* counterions ground state configurations as a function of the number of *overcharging* counterions  $n$ : (a)  $Z_m = 60$ ,  $Z_c = 2$  (b)  $Z_m = 60$ ,  $Z_c = 3$  (c)  $Z_m = 180$ ,  $Z_c = 2$  (d)  $Z_m = 180$ ,  $Z_c = 3$ . Overcharge curves were computed for discrete macroion charge distribution (DCC) and central macroionic charge (CC). The neutral case was chosen as the potential energy origin. Dashed lines were produced by using equation (16). For discrete systems (DCC) error bars are only indicated when larger than symbols.

some<sup>6</sup> of these free DCC sites. Figure 8 shows that overcharging is significantly less affected by colloid charge discretization for multivalent counterions compared to monovalent counterion systems (see Fig. 7), and this, the higher the counterion valence  $Z_c$  and the macroion charge  $Z_m$ .

For the discrete system with  $Z_m = 60$ , simulations show that overcharging can even be stronger, regarding the energy gain as well as  $n^*$ , than in the continuous case [see Figs. 8(a) and (b)]. This phenomenon can be qualitatively understood by referring to the low macroion surface charge density limit. In-

<sup>6</sup> It can be one or more depending on the valence, surface charged density and the local DCC site arrangement.

deed, for sufficient low  $Z_m$  (macroion area  $A$  being fixed) and/or sufficient high  $a$  ( $Z_m$  being fixed), the correlation term  $\Delta E_n^{cor}$  (corresponding to the continuous case) in Eq. (16) is negligible compared to the ionic pairing term  $E_{pin}$  given by Eq. (9). Thereby, for very low charge density and fixed  $Z_c$ , all repulsive counterion-counterion interactions become negligible compared to  $E_{pin}$ . In this limiting situation the overcharging energy gain is approximatively given by  $-nZ_dZ_c/d_{pin}$ , so that *full* overcharging occurs where each monovalent DCC site is paired with one (multivalent) counterion. It turns out, that for these specific simulation parameters  $Z_m = 60$ ,  $a = 8\sigma$ ,  $Z_c = 2$  and  $3$  involved in Figs. 8(a) and (b), the corresponding DCC site concentration is sufficiently low to produce a stronger overcharge than the one obtained with a central charge.

For high enough  $Z_m$  (here  $Z_m = 180$ ), the overcharging curves, for discrete and continuous systems depicted in Figs. 8(c-d), are almost identical and a fortiori quasi identical to the one predicted by WC theory through Eq. (16). This is consistent with what we already found in Sec. 3.2.2 for the counterion structure in neutral state, where we showed that, for  $Z_m = 180$ ,  $g_c^{(DCC)}(r)$  approaches  $g_c^{(CC)}(r)$  with increasing  $Z_c$ . However, the agreement between discrete and continuous cases is even better for overcharging properties than for counterion structure [see the corresponding  $g_c(r)$  given in Figs. 5(c) and (d)]. This is due to the fact that, as previously mentioned, the WC approach quantifying overcharging energy gain by Eq. (16) is already excellent for highly short-ranged ordered systems. Generally speaking, all the ordering mechanisms related in Sec. 3.1 for neutral discrete systems hold for the overcharging features: *all causes leading to ordering enhance overcharging*.

## 4 Finite temperature

In this part, the system is globally *neutral* and is brought to room temperature  $T_0$ . We are interested in determining the counterions distribution as well as the counterion motion within the counterion layer. The cell radius  $R$  is fixed to  $40\sigma$  so that the macroion volume fraction  $f_m$  has the *finite* value  $8 \times 10^{-3}$ .

### 4.1 Strong Coulomb coupling

The Bjerrum length  $l_B$  is set to  $10\sigma$  as previously in the ground state study Sec. 3.1. In this section we consider two macroion bare charges  $Z_m$  (60 and 180) and three counterion valences  $Z_c$  (1, 2 and 3). A typical parameter for describing the Coulomb coupling strength is  $\Gamma$  [22] defined as  $\Gamma = l_B Z_c^2 / \tilde{a}_{cc}$ . For these simulation parameters,  $\Gamma$  ranges from 2.6 (for  $Z_m = 60$  and  $Z_c = 1$ )

to 23.1 (for  $Z_m = 180$  and  $Z_c = 3$ ). Under these conditions, systems are still highly energy dominated so that at equilibrium almost all (if not all depending on  $Z_m$  and  $Z_c$ ) counterions lie at the vicinity of the macroion surface (strong condensation). Therefore for the strong Coulomb coupling regime, it is suitable to focus on the counterion *surface* properties (here distribution and diffusion).

#### 4.1.1 Counterion distribution

Like in the ground state analysis, we characterize the counterion distribution via its surface correlation function. At non zero temperature, correlation functions are computed by averaging  $\sum_{i \neq j} \delta(r - r_i) \delta(r - r_j)$  over 1000 independent equilibrium configurations which are statistically uncorrelated.

Results for monovalent counterions are depicted in Fig. 9(a) and 9(b) for  $Z_m = 60$  and  $Z_m = 180$  respectively. For both charges  $Z_m$  the counterion distributions are weakly affected by charge discretization and  $g_c^{(DCC)}(r)$  and  $g_c^{(CC)}(r)$  curves are almost identical [see Fig. 9(a) and Fig. 9(b)]. A closer look on Fig. 9(a) and Fig. 9(b), reveal that the agreement between discrete and continuous systems is even better for high macroion charge density ( $Z_m = 180$ ) as expected. In fact, for monovalent systems, the pinning term  $E_{pin}$ , mainly governed by Eq. (9), has its lowest magnitude and entropic effects can sufficiently *locally disorder* the compact ionic pair configuration. In particular, when  $\sigma_m$  is sufficient high, the *fluctuating* intra-dipole separation becomes comparable to the inter-dipole separation and discretization effects (i. e. pinning) are canceled. These pinning and unpinning aspects will be addressed in more details in the next section 4.2. As expected, the counterion positional

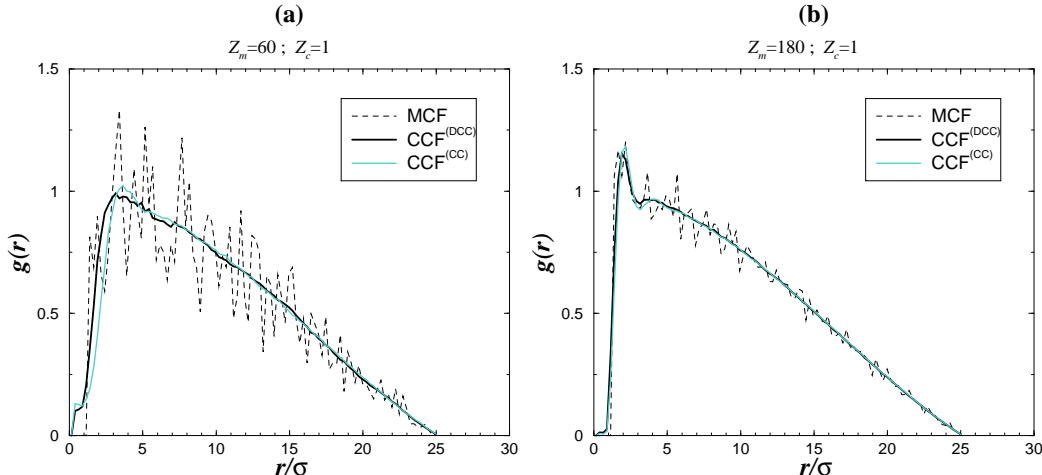


Fig. 9. Surface correlation functions at room temperature  $T_0$  for *monovalent* counterions. The two counterion correlation functions (CCF)  $g_c(r)$  are obtained for discrete colloidal charges (DCC) and for the central charge (CC): (a)  $Z_m = 60$  (b)  $Z_m = 180$ . MCF stands for  $g_m(r)$ .

order, for discrete and continuous cases, is much weaker at room temperature than in the ground state case (compare Fig. 9 and Fig. 2).

Results for multivalent counterions are depicted in Fig. 10. It clearly shows that now the counterion distributions are strongly affected by charge discretization, and this, the higher  $Z_c$ . This is in contrast with what was found in the ground state analysis Sec. 3.1.2 where no counterion motion occurs. This effect is of course due to the pinning (inhibition of large counterion motion), mainly governed by Eq. (9), which is proportional to  $Z_c$ .

Note that all these above statements hold for the particular finite temperature  $T_0$ . However the effect of finite temperature discussed here should hold, at least qualitatively, for a large temperature range. For very low temperature

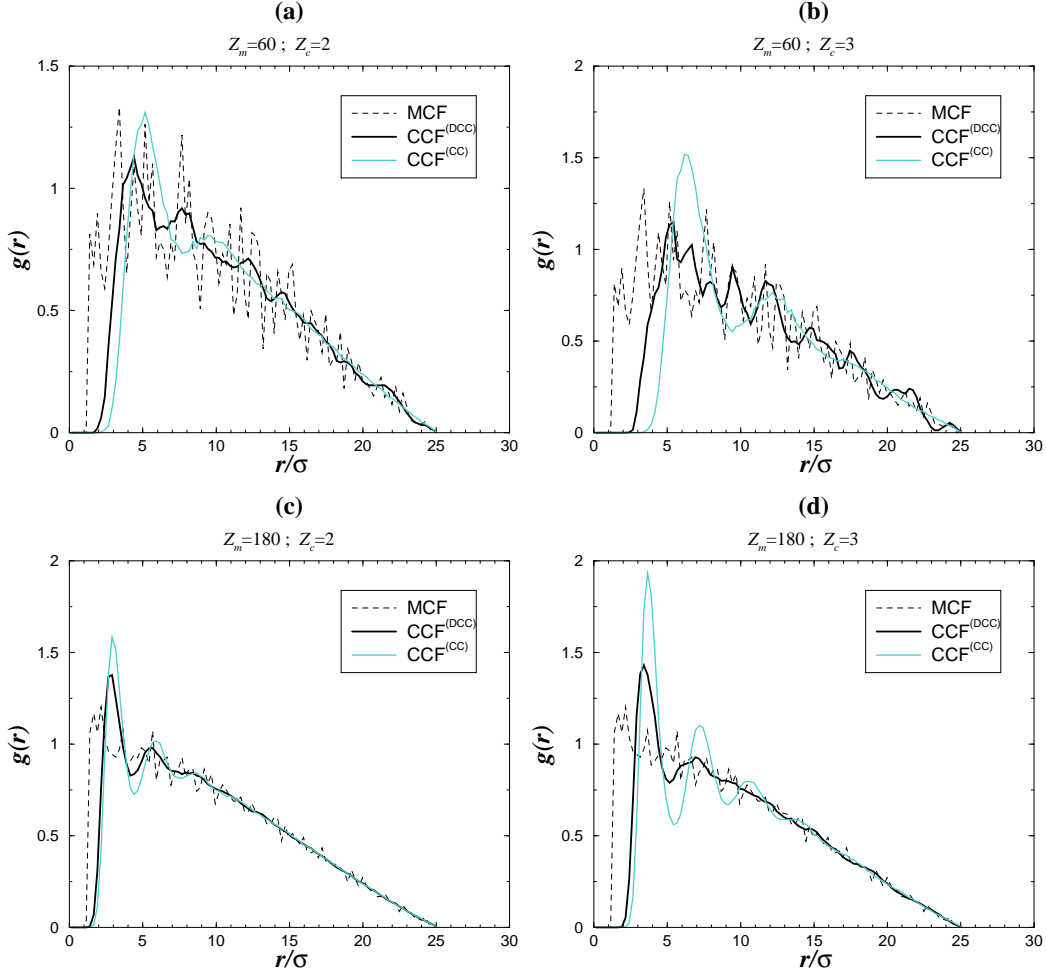


Fig. 10. Surface correlation functions at room temperature  $T_0$  for *multivalent* counterions. The two counterion correlation functions (CCF)  $g_c(r)$  are obtained for discrete colloidal charges (DCC) and for the central charge (CC): (a)  $Z_m = 60$ ,  $Z_c = 2$  (b)  $Z_m = 60$ ,  $Z_c = 3$  (c)  $Z_m = 180$ ,  $Z_c = 2$  (d)  $Z_m = 180$ ,  $Z_c = 3$ . MCF stands for  $g_m(r)$ .

one should recover all ground state properties mentioned in the ground state study Sec. 3.1.

#### 4.1.2 Surface diffusion

This section is devoted to answer the following question: do the counterions only oscillate around the DCC sites or do they have also a large translational motion over the sphere?

To study this problem one introduces the following observable:

$$\Delta x^2(t, t_0) = \frac{1}{t - t_0} \int_{t_0}^t dt' [x(t') - x(t_0)]^2, \quad (18)$$

which is referred as the *mean square displacement* (MSD), where  $x(t_0)$  represents the position of a given counterion at time  $t = t_0$  (at equilibrium) and  $x(t, t_0)$  is its position at later time  $t$ . This observable is suitable for the strong Coulomb coupling where quasi-all particles (if not all depending on  $Z_m$  and  $Z_c$ ) lie at the vicinity of the sphere. All particles lying within a distance  $9.2\sigma$  from the macroion center are radially projected on the macroion surface of radius  $a = 8\sigma$  to give  $x(t, t_0)$ . The root mean square displacement (RMSD)  $\Delta x(t, t_0)$  is defined as

$$\Delta x(t, t_0) = \sqrt{\Delta x^2(t, t_0)}. \quad (19)$$

Like for the surface correlation function, the RMSD is measured on the spherical surface (arc length) and it has a natural upper limit  $\pi a$ . For the case of free counterions (i. e. central charge case without pinning) the RMSD  $\Delta x_{free}$  reads

$$\Delta x_{free} = a \sqrt{\frac{\pi^2 - 4}{2}} \approx 13.7\sigma. \quad (20)$$

This quantity  $\Delta x_{free}$  will be useful to refer to the “unpinned” state.

Results for discrete systems are sketched in Fig. 12(a) and Fig. 12(b) for  $Z_m = 60$  and  $Z_m = 180$  respectively, where each counterion’ RMSD is given. For monovalent counterions, they are free to move over the macroion surface for both bare charges  $Z_m$  considered here. Moreover, our simulation data show that, for fixed  $Z_m$ , the counterions become gradually pinned with increasing  $Z_c$ . All these features are captured by the  $Z_c$  dependency of the pinning term  $E_{pin}$ . For multivalent counterions, the degree of pinning increases with decreasing  $Z_m$  for fixed  $Z_c$ . This is due to the fact that discrete charges become closer

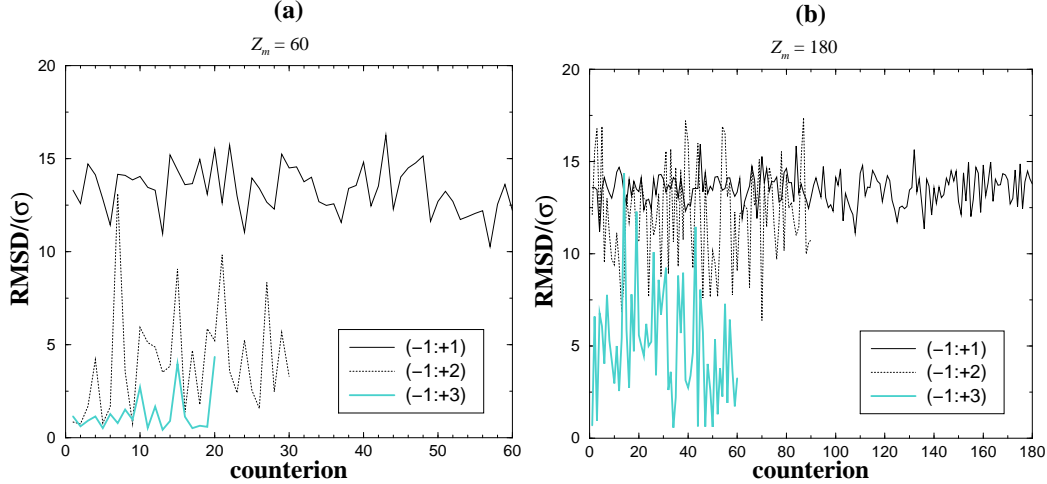


Fig. 11. Root mean square displacement (RMSD) for each counterion and for different valences  $Z_c$ . (a)  $Z_m = 60$  (b)  $Z_m = 180$ .

from each other by increasing  $\sigma_m$  (i. e.  $Z_m$ ) so that energetically a counterion jump from site to site is less demanding. For the continuous case, we have checked that, for the same parameters, counterions have always a large lateral motion and can move all over the sphere.

#### 4.2 Moderate Coulomb coupling

In this last part, the Bjerrum length corresponds to that of water at room temperature ( $l_B = 2\sigma = 7.14 \text{ \AA}$ ). For this moderate Coulomb coupling counterions occupy *all* the cell volume. Clearly, the probability of finding counterions plainly outside the macroion surface is *nomore* negligible (in contrast with the strong Coulomb coupling). The target quantity is the fraction  $P(r)$  of counterions lying within a distance  $r$  from the macroion center, defined as

$$P(r) = N(r)/N_c \quad (21)$$

with

$$N(r) = \int_{r_0}^r 4\pi r_i^2 c_v(r_i) dr_i, \quad (22)$$

where  $c_v(r)$  is the counterion *volume* concentration profile. As usual,  $N(r)$ , also called integrated charge, is averaged in the canonical ensemble.

Results for  $Z_m = 60$  and  $Z_m = 12$  are sketched in Fig. 12(a) and Fig. 12(b) respectively, and this, for different counterion valences. For the highest charge,

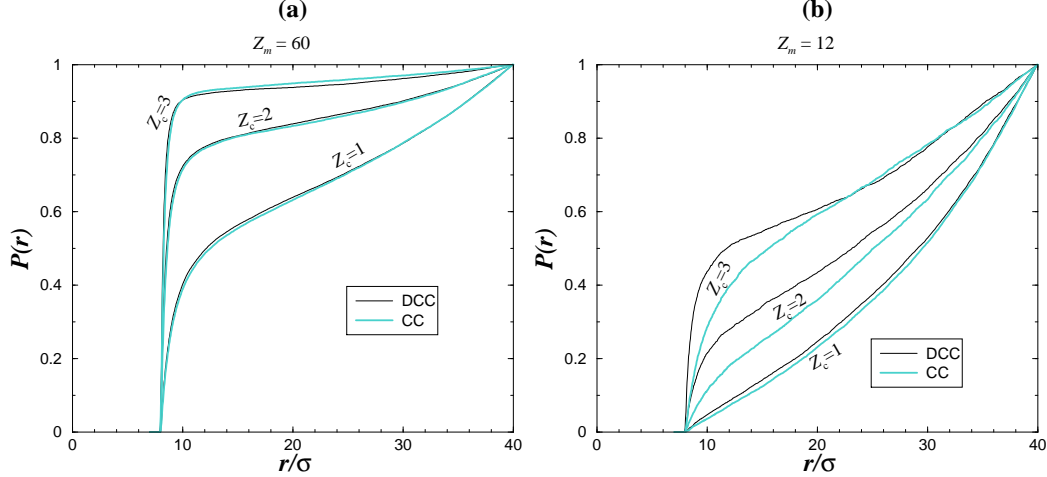


Fig. 12. Counterion fraction within a distance  $r$  from the macroion center for different valences  $Z_c$ . (a)  $Z_m = 60$  (b)  $Z_m = 12$ . Data were computed for discrete macroion charge distribution (DCC) and central macroionic charge (CC).

Fig. 12(a) shows that discretization effects are canceled for all valences. In return, for the small charge density case, Fig. 12(b) shows that discretization effects become important for multivalent counterions. In the present situation, the Coulomb coupling is five times less important than in the strong coupling case studied in Sec. 4.1, therefore pinning effects discussed previously, can only be noticeable for sufficient low  $\sigma_m$  (here  $Z_m = 12$ ) and multivalent counterions.

## 5 Concluding remarks

We have performed MD simulations within the framework of the primitive model to study the coupled effects of macroion charge discretization and counterion valence. The macroion bare charge is carried by monovalent microions randomly distributed over the colloidal surface. Different correlational regimes were considered: (i) ground state and (ii) finite temperature.

Concerning the ground state analysis (i), we were interested in the counterion structure in the neutral state and the overcharging phenomenon. We demonstrated, that counterion structure order (counterion structure disorder induced by the discrete random macroion charge distribution) is increased (decreased) by increasing macroion surface charge density  $\sigma_m$  and/or counterion valence  $Z_c$ . For monovalent counterions, we showed that the ratio between the DCC-counterion distance of closest approach and mean distance between counterions is a fundamental quantity to describe counterion ordering. When overcharge comes into play, similar effects occur. More precisely, for sufficiently high charge density  $\sigma_m$  the overcharging is *quantitatively* the same as the one obtained in the continuous case (central charge), and this, for monovalent as

well as multivalent counterions. For low  $\sigma_m$ , the overcharging can even be stronger in the discrete case than in the continuous case for multivalent counterions. In return, for monovalent counterions overcharge is always weaker than in the continuous case but approaches the later with increasing  $\sigma_m$ .

In the finite temperature case (ii) strong and moderate Coulomb couplings were addressed. In the strong Coulomb coupling, we showed that counterion pinning increases with increasing  $Z_c$  and decreasing  $\sigma_m$  as one can intuitively guess. In the moderate Coulomb coupling corresponding to an aqueous situation, the *volume* counterion distribution is only affected for low  $\sigma_m$  and multivalent counterions.

A future work will address the presence of added salts.

## Acknowledgements

I thank C. Holm, A. Johner, K. Kremer and B. Shklovskii for helpful discussions. H. Schiessel is acknowledged for a careful reading of the manuscript. This work is supported by *Laboratoires Européens Associés* (LEA).

## References

- [1] J. Israelachvili, *Intermolecular and Surface Forces*, Academic, London, 1992.
- [2] D. F. Evans, H. Wennerström, *The Colloidal Domain*, Wiley-VCH, New York, 1999.
- [3] T. L. Hill, *Statistical mechanics*, Addison-Wesley, Reading, Mass., 1960.
- [4] H. Wennerström, B. Jönsson, P. Linse, *J. Chem. Phys.* 76 (1982) 4665–4670”.
- [5] V. Perel, B. Shklovskii, *Physica* 274A (1999) 446–452.
- [6] B. Shklovskii, *Phys. Rev. E* 60 (1999) 5802–5810.
- [7] E. M. Mateescu, C. Jeppesen, P. Pincus, *Europhys. Lett.* 46 (1999) 493–498.
- [8] J. F. Joanny, *Europ. J. Phys. B* 9 (1999) 117–122.
- [9] E. Gurovitch, P. Sens, *Phys. Rev. Lett.* 82 (1999) 339–342.
- [10] M. Lozada-Cassou, E. González-Tovar, W. Olivares, *Phys. Rev. E* 60 (1999) R17–R20.
- [11] M. Deserno, C. Holm, S. May, *Macromolecules* 33 (2000) 199–206.

- [12] R. Messina, C. Holm, K. Kremer, *Phys. Rev. Lett.* 85 (2000) 872–875.
- [13] R. Messina, C. Holm, K. Kremer, *Europhys. Lett.* 51 (2000) 461–467.
- [14] T. T. Nguyen, A. Y. Grosberg, B. I. Shklovskii, *Phys. Rev. Lett.* 85 (2000) 1568–1571.
- [15] T. T. Nguyen, A. Y. Grosberg, B. I. Shklovskii, *J. Chem. Phys.* 113 (2000) 1110–1125.
- [16] R. Messina, C. Holm, K. Kremer, *Eur. Phys. J. E* 4 (2001) 363–370.
- [17] R. Messina, C. Holm, K. Kremer, *Phys. Rev. E* 64 (2001) 021405.
- [18] O. Spalla, L. Belloni, *J. Chem. Phys.* 95 (1991) 7689–7697.
- [19] S. Bhattacharjee, C. H. Ko, M. Elimelech, *Langmuir* 14 (1998) 3365–3375.
- [20] K. S. Schmitz, *Langmuir* 15 (1999) 2854–2684.
- [21] L. Bonsall, A. A. Maradudin, *Phys. Rev. B* 15 (1977) 1959–1973.
- [22] I. Rouzina, V. A. Bloomfield, *J. Chem. Phys.* 100 (1996) 9977–9989.